AD-A183 073 NONLINEAR THEORY OF THE ORBITRON MASER IN THREE-DIMENSIONS(U) NAVAL RESEARCH LAB WASHINGTON DC A K GANGULY ET AL 30 JUN 87 NRL-MR-5979 1/1

UNCLASSIFIED F/G 9/3 NL

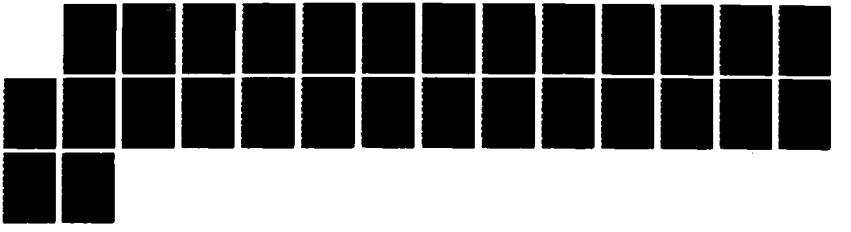

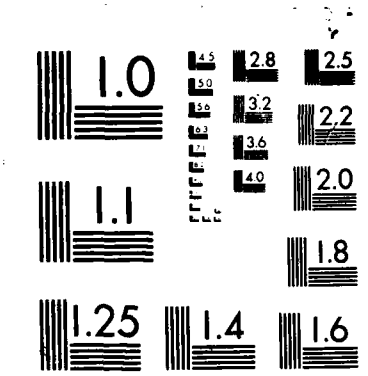

NRL Memorandum Report 5979

Nonlinear Theory of the Orbitron Maser in Three-Dimensions

A. K. GANGULY, H. P. FREUND, AND S. AHN

Microwave and Millimeter Wave Tube Technology Branch
Electronics Technology Division

June 30, 1987

SECURITY CLASSIFICATION OF THIS PAGE

REPORT DOCUMENTATION PAGE

1a REPORT SECURITY CLASSIFICATION UNCLASSIFIED	1b RESTRICTIVE MARKINGS AD-A183072
2a SECURITY CLASSIFICATION AUTHORITY	3 DISTRIBUTION/AVAILABILITY OF REPORT Approved for public release; distribution unlimited.
2b DECLASSIFICATION/DOWNGRADING SCHEDULE	
4 PERFORMING ORGANIZATION REPORT NUMBER(S) NRL Memorandum Report 5979	5 MONITORING ORGANIZATION REPORT NUMBER(S)
6a NAME OF PERFORMING ORGANIZATION Naval Research Laboratory 6b OFFICE SYMBOL (If applicable) Code 6840	7a NAME OF MONITORING ORGANIZATION
6c ADDRESS (City, State, and ZIP Code) Washington, DC 20375-5000	7b ADDRESS (City, State, and ZIP Code)
8a NAME OF FUNDING/SPONSORING ORGANIZATION 8b OFFICE SYMBOL (If applicable)	9 PROCUREMENT INSTRUMENT IDENTIFICATION NUMBER
8c ADDRESS (City, State, and ZIP Code)	10 SOURCE OF FUNDING NUMBERS PROGRAM ELEMENT NO. / PROJECT NO / TASK NO / WORK UNIT ACCESSION NO

11 TITLE (Include Security Classification)
Nonlinear Theory of the Orbitron Maser in Three-Dimensions

12 PERSONAL AUTHOR(S)
Ganguly, A.K., Freund,* H.P., and Ahn, S.

13a TYPE OF REPORT	13b TIME COVERED FROM _____ TO _____	14 DATE OF REPORT (Year, Month, Day)	15 PAGE COUNT
		1987 June 30	28

16 SUPPLEMENTARY NOTATION
*Permanent Address: Science Applications International Corp., McLean, VA 22102

17 COSATI CODES			18 SUBJECT TERMS (Continue on reverse if necessary and identify by block number)
FIELD	GROUP	SUB-GROUP	Orbitron Maser

19 ABSTRACT (Continue on reverse if necessary and identify by block number)

The nonlinear analysis of the Orbitron Maser is studied numerically for an amplifier configuration in which an electron beam propagates through a coaxial waveguide with a voltage applied between the inner and outer conductors. A set of coupled nonlinear differential equations is derived in three-dimensions which governs the self-consistent evolution of either the TE, TM, or TEM modes in a loss-free coaxial waveguide as well as the trajectories of an ensemble of electrons. The saturation efficiency as well as the linear growth rate are calculated and, although the linear growth rate for the orbitron amplifier is moderately high ($\sim 1.0 dB/cm$), the efficiency is low ($\lesssim$ 6.1%). Severe limitations arise in the high frequency operation of the orbitron amplifier in the fundamental mode due to the break-down electric field and extremely small radius of the inner conductor.

20 DISTRIBUTION/AVAILABILITY OF ABSTRACT	21 ABSTRACT SECURITY CLASSIFICATION
☒ UNCLASSIFIED/UNLIMITED ☐ SAME AS RPT ☐ DTIC USERS	UNCLASSIFIED
22a NAME OF RESPONSIBLE INDIVIDUAL Saeyoung Ahn	22b TELEPHONE (Include Area Code) (202) 767-3382 / 22c OFFICE SYMBOL Code 6841

DD FORM 1473, 84 MAR 83 APR edition may be used until exhausted
All other editions are obsolete

SECURITY CLASSIFICATION OF THIS PAGE

☆U.S. Government Printing Office: 1985-607-047

CONTENTS

NONLINEAR THEORY OF THE ORBITRON MASER IN THREE-DIMENSIONS

I. INTRODUCTION

An early application in which electrostatic focussing was used to impart a periodic oscillation on electron trajectories was by Watkins and Wada[1] who employed a coaxial waveguide in which the central element was a four-conductor transmission line. A dc voltage applied between the inner and outer conductors gave rise to a radial electric field which balances the centrifugal force on the electrons and permits orbital motion about the central conductor. Maser amplification is possible when the rotational phase of the electrons is in synchronism with the phase of the waveguide modes of the system. Recently Alexeff and Dyer[2] have conducted an extensive series of experiments for a configuration in which the central conductor was a single wire, and emission was found at relatively low efficiency (an optimized experiment found emission at *30 GHz* with an *efficiency of about 5%)*.

Numerous theoretical analyses of the linear stability of the interaction have been conducted based upon a perturbation about an equilibrium in which the electrons execute circular trajectories about the central conductor and the bulk beam is an annulus.[2-6] These studies have shown that the Orbitron maser has the potential for producing extremely large growth rates (i.e., short e-folding lengths).[3,4] However, the difficulty encountered with configurations based upon circular electron trajectories is that high frequency operation (> 30 GHz) requires relatively high voltages. In order to circumvent this problem, Burke et al[7] proposed a configuration in which the trajectories are highly eccentric ellipses in which the electrons pass extremely close to the central conductor. In such cases, resonant interactions with large growth rates can occur at relatively high frequencies for moderate voltages if the central wire is thin and the orbital eccentricity is high.

Manuscript approved March 5, 1987.

While the linear theory of the Orbitron Maser has been amply studied, no nonlinear analyses have heretofore appeared which provide estimates of the interaction efficiencies. It is our purpose in this paper to develop a fully three-dimensional nonlinear analysis of the Orbitron Maser to study the evolution of the system through the linear regime of the interaction to saturation. This study will lead to an accurate calculation of the interaction efficiency in Orbitron Maser and a realistic assessment of its potential as a high power and high efficiency amplifier, particularly at high frequencies. To this end, a set of nonlinear coupled differential equations is derived in Sec II which governs the self-consistent evolution of either the TE, TM or TEM modes as well as the trajectories of an ensemble of electrons. Further, the electron trajectories are treated in sufficiently general manner as to include arbitrary eccentricities, hence we treat both circular and elliptic orbits. Boundary conditions appropriate for either the TE, TM or TEM modes are applied to treat the effects of the finite waveguide geometry. The space charge effects are neglected in the analysis and it will be applicable in the tenuous beam limit. The nonlinear dispersion relation derived in Sec II, however, includes collective effects through the dielectric response of the plasma to the waveguide mode. In addition, since we are interested in the amplifier configuration, only single mode propagation is considered. This permits an average over a wave period to be performed which eliminates the fast-time scale phenomena from the formulation and results in an increase in the computational efficiency. The numerical solution of the coupled equations in given in Sec III for a few sample cases. The efficiency of the amplifier is found to be small ($\lesssim 6\%$). The constraints which appear in the orbitron amplifier operation at high frequency due to the break-down electric field and the requirement of an extremely thin inner conductor wire are also discussed. A summary and discussion are given in Sec IV, where efficiency enhancement schemes are indicated.

II. PHYSICAL MODEL: GENERAL EQUATIONS

The physical configuration we employ is shown in Fig. 1. It consists of an axis encircling electron beam propagating axially through a coaxial waveguide of circular cross-section with inner radius r_1 and outer radius r_2. The electrons are radially confined by balancing the centrifugal force against the radial electric field produced by applying a dc voltage between the two conductors. If the space charge effects are neglected, then the dc electrostatic potential in the configuration of Fig. 1 is given by

$$\phi(r) = -\frac{V_0}{ln(r_2/r_1)}\, ln\ (r/r_1) \tag{1}$$

and the d.c. electric field is

$$\mathbf{E}_0\ (\mathbf{r}) = \frac{V_0}{ln(r_2/r_1)} \cdot \frac{1}{r}\, \hat{\mathbf{e}}_r \tag{2}$$

where $\hat{\mathbf{e}}_r$, $\hat{\mathbf{e}}_\theta$, and $\hat{\mathbf{e}}_z$ denote the unit vectors in r,θ and z coordinates, respectively.

(a) Equilibrium Orbits

The charateristics of the steady-state orbits of the electrons acted on by the conservative potential $\phi(r)$ in Eq. (1) were calculated by Burke at al[7] in the nonrelativistic limit. The relativistic Lagrangian is given by

$$L = -m_o c^2 \left\{1 - \frac{1}{c^2}\ (\dot{r}^2 + r^2\, \dot{\theta}^2 + \dot{z}^2)\right\}^{1/2} + e\phi, \tag{3}$$

where m_0 and e are, respectively, the rest mass and the magnitude of the charge of an electron. Here $c = 1/\sqrt{u_0\epsilon_0}$ is the speed of light in vacuum, μ_0 is the vacuum permeability and ϵ_0 is the vacuum dielectric constant. In Eq. (3), the dot over a quantity denotes time derivative. The Hamiltonian is

$$H = m_0\, c^2\, \gamma - e\, \phi, \tag{4}$$

where

$$\gamma = \left\{1 - \frac{1}{c^2}\ (\dot{r}^2 + r^2\, \dot{\theta}^2 + \dot{z}^2)\right\}^{-1/2} \tag{5}$$

Since, the Lagrangian does not involve time explicity and is independent of θ and z, the three constants of motion for the steady-state orbits are H, P_z and P_θ where

$$P_\theta = r\ p_\theta = m_o\ \gamma\ r^2\ \dot{\theta}, \tag{6a}$$

$$P_z = m_0\, \gamma\, \dot{z}, \tag{6b}$$

$$H = m_0\, c^2 \left\{1 + \frac{1}{m_0^2\, c^2}\left[p_z^2 + \frac{P_\theta^2}{r^2} + p_r^2\right]\right\}^{1/2} + \frac{eV_0}{ln(r_2/r_1)}\, ln\ \frac{r}{r_1}. \tag{6c}$$

In Eqs 6c, $p_r = m_0\, \gamma \dot{r}$. The angular momentum term in Eq. (6c) provides an outward radial force which dominates at small r and the electrostatic potential provides an inward force which dominates at large r. Thus the orbits have an inner and outer radial turning point,[7] r_{in} and r_{out}, respectively. Since p_r is zero at each turning point, r_{in} and r_{out} are the roots of the equation

$$c\ p_r = \left\{\left[H - \frac{eV_0}{ln(r_2/r_1)}\ ln\frac{r}{r_1}\right]^2 - m_0^2\ c^4 - c^2\ p_z^2 - \frac{c^2 P_\theta^2}{r^2}\right\}^{1/2} = 0. \tag{7}$$

For the special case of circular orbits ($r_{in} = r_{out} = r_0$) both p_r and $\dot{p}_r = -\frac{\partial H}{\partial r}$ are zero. Thus, from Eqs. (6a) and (6c), we obtain the following relation between the azimuthal rotation frequency Ω_θ and the radius r_0

$$\Omega_\theta = \dot{\theta} = \frac{c}{r_0}\sqrt{\frac{eV_0/\gamma\ m_0 c^2}{ln(r_2/r_1)}}. \tag{8}$$

In the nonrelativistic case,[7] Eqs. (7) and (8), respectively, take the forms

$$H_0 - \frac{P_z^2}{2m_0} - \frac{P_\theta^2}{2m_0 r^2} - \frac{eV_0}{ln(r_2/r_1)}\ ln\frac{r}{r_1} = 0, \tag{7a}$$

and

$$\Omega_\theta = \frac{c}{r_0}\sqrt{\frac{eV_0/m_0\ c^2}{ln(r_2/r_1)}}, \tag{8a}$$

where $H_0 = H - m_0\ c^2$. In Ref. (7), it is shown that the characteristics of the equilibrium orbits in the nonrelativistic case can be described by a single parameter

$$\sigma = r_{out}/r_{in} \tag{9}$$

for given values of the constants H, p_z and P_θ. When $\sigma \neq 1$, the two characteristic frequencies Ω_r (the radial oscillation frequency) and Ω_θ (azimuthal oscillation frequency) are expressed as integrals for which there are no closed form solutions. An electromagnetic wave can interchange energy with an electron near synchronous condition $\omega = l\ \Omega_\theta + n\ \Omega_r + k v_z$, where ω is the wave frequency, k the wave vector and v_z, the axial velocity of the electons.

(b) RF Fields:

The coaxial waveguide can propagate TE, TM or TEM modes. The lowest order mode is TEM where the electric field is radial. Therefore, the TEM mode cannot exchange energy with electrons moving in circular orbits TE or TM modes, however, can interact with electrons in circular orbits. The radiation field will be determined by solving the Maxwell's equations for the vector potential $\delta\ \mathbf{A}\ (\mathbf{r},t)$

$$\nabla^2\ \delta\ \mathbf{A} - \frac{\partial^2\ \delta\ \mathbf{A}}{\partial t^2} = -\mu_0\ \delta\ \mathbf{J}\ (\mathbf{r},t), \tag{10}$$

subject to the auxillary condition $\nabla \cdot \delta\ \mathbf{A} = 0$. In Eq. (10) $\delta\ \mathbf{J}$ is the source current. Since the space charge fields are neglected, the boundary conditions at the waveguide wall can be satisfied by expanding

the vector potential in terms of the orthonormal basis functions of the empty guide. Thus, we write the vector potential of the radiation field for TE modes in the form

$$\delta \mathbf{A}(\mathbf{r},t) = \frac{1}{2} \sum_{l,n} \delta A_{ln}(z)\, \mathbf{e}_{ln}(r,\theta)\, e^{i\left(\int k(z)dz - \omega t\right)} + c.c. \tag{11}$$

The transverse basis functions $\mathbf{e}_{ln}$ in Eq. (11) are represented by

$$\mathbf{e}_{ln}(r,\theta) = C_{ln}\, k_{ln} \left\{ \hat{\mathbf{e}}_\theta\, Z_{ln}(k_{ln} r) - \frac{il}{k_{ln} r}\, \hat{\mathbf{e}}_r\, Z_{ln}(k_{ln} r) \right\} e^{il\theta}, \tag{12}$$

where

$$Z_{ln}(r) = J_{ln}(k_{ln} r) - \frac{J_{ln}(k_{ln} r_1)}{Y_{ln}(k_{ln} r_1)}\, Y_{ln}(k_{ln} r), \tag{13}$$

and J_{ln} and Y_{ln} are, respectively, the l-th order Bessel functions of the first and the second kind. Z_{ln}', J_{ln}' and Y_{ln}' denote, respectively, the first derivative of Z_{ln}, J_{ln} and Y_{ln}. k_{ln}s are the roots of the equation

$$Z_{ln}'(k_{ln}\, r_2) = 0, \tag{14}$$

and the normalization constant C_{ln} is

$$C_{ln} = \frac{1}{\pi^{1/2}} \left\{ \frac{1}{(x_2^2 - l^2)\, Z_{ln}^2(x_2) - (x_1^2 - l^2)\, Z_{ln}^2(x_1)} \right\}^{1/2}, \tag{15}$$

where $x_i = k_{ln} r_i$. The basis functions satisfy the orthonormal property

$$\int_{A_c} \mathbf{e}_{ln} \cdot \mathbf{e}_{l'n'}^{*}\, dS = \delta_{ll'}\, \delta_{nn'}, \tag{16}$$

where $A_c = \pi(r_2^2 - r_1^2)$ is the cross-sectional area of the waveguide. It is assumed that the mode amplitude and the wave vector $k(z)$ are both slowly varying functions of z such that $\frac{d}{dz}[\ln \delta A(z)] << k$ and $\frac{d}{dz}[\ln k(z)] << k$.

For TM modes, the vector potential is given by

$$\delta \mathbf{A}(\mathbf{r},t) = \frac{1}{2} \sum_{l,n} \delta A_{ln}(z) \left\{ \mathbf{e}_{ln}^{(t)} - \frac{ik_{ln}}{k}\, \mathbf{e}_{ln}^{(z)} \right\} e^{i\left(\int k(z)dz - \omega t\right)} + c.c., \tag{16}$$

where the transverse and the longitudinal basis functions are respectively,

$$\mathbf{e}_{ln}^{(t)} = C_{ln}\, k_{ln} \left[\hat{\mathbf{e}}_r\, Z_{ln}'(k_{ln} r) + \frac{il}{k_{ln} r}\, Z_{ln}(k_{ln} r)\, \hat{\mathbf{e}}_\theta \right] e^{il\theta}, \tag{17}$$

and

$$\mathbf{e}_{ln}^{(z)} = \hat{\mathbf{e}}_z\, C_{ln}\, k_{ln}\, Z_{ln}(k_{ln} r)\, e^{il\theta} \tag{18}$$

In Eqs. (16)-(18), k_{ln} are the roots of the equation

$$Z_{ln}(k_{ln} r_2) = 0, \tag{19}$$

where

$$Z_{ln} = J_l(k_l\ r) - \frac{J_l(k_{ln} r_1)}{Y_l(k_{ln} r_1)}\ Y_l(k_{ln} r). \tag{20}$$

The normalization constant C_{ln} for TM modes is given by

$$C_{ln} = \frac{1}{\pi^{1/2}} \cdot \left\{ \frac{1}{x_2^2\ Z_{ln}'^2(x_2) - x_1^2\ Z_{ln}'^2(x_1)} \right\}^{1/2}, \tag{21}$$

such that

$$\int_{A_g} \mathbf{e}_{ln}^{(t)} \cdot \mathbf{e}_{l'n'}^{(t)*}\, ds = \delta_{ll'}\ \delta_{nm'}, \tag{22}$$

and

$$\int_{A_g} \mathbf{e}_{ln}^{(z)} \cdot \mathbf{e}_{l'n}^{(z)*}\, ds = \delta_{ll'}\ \delta_{nm}.$$

The vector potential of the wave field for TEM modes may be written as

$$\delta\ \mathbf{A}(\mathbf{r},t) = \frac{1}{2}\ \mathbf{e}_{\mathrm{TEM}}\ \delta\ A(z) e^{i\left(\int k(z)dz' - \omega t\right)} + c.c. \tag{23}$$

where

$$\mathbf{e}_{\mathrm{TEM}} = \hat{\mathbf{e}}_r\ \frac{1}{\sqrt{2\pi\, ln(r_2/r_1)}} \cdot \frac{1}{r} \tag{24}$$

such that

$$\int_{A_g} \mathbf{e}_{\mathrm{TEM}} \cdot \mathbf{e}_{\mathrm{TEM}}\, dS = 1. \tag{25}$$

The vector potential for TE (Eq. 11) and TEM (Eq. 23) modes satisfy the condition $\nabla \cdot \mathbf{A} = 0$ exactly whereas TM modes (Eq. 16) satisfy this relation if the variation of δA_{ln} with z is ignored.

The microscopic source current, $\delta\mathbf{J}$, can be written as the sum over individual particle trajectories

$$\delta\mathbf{J}(\mathbf{r},t) = -\ e\ n_b\ \frac{L}{N_T} \sum_{j=1}^{N_T} \mathbf{v}_j\ (z, \mathbf{x}_{j0}, t_{j0})\ \frac{\delta(t - \tau_j(z, \mathbf{x}_{j0}, t_{j0}))}{|v_{zj}\ (z, \mathbf{x}_{j0}, t_{j0})|}\ \delta(\mathbf{x} - \mathbf{x}_j\ (z, \mathbf{x}_{j0}, t_{j0})) \tag{26}$$

where $\mathbf{v}_j(z, \mathbf{x}_{j0}, \mathbf{t}_{j0})$ is the velocity of the j-th electron at position z which entered the interaction region at time t_{j0} and the transverse position $\mathbf{x}_{j0}$ and

$$\tau_j(z, \mathbf{x}_{j0}, t_{j0}) = t_{j0} + \int_0^{z} \frac{dz'}{v_{zj}\ (z, \mathbf{x}_{j0}, t_{j0})}.$$

The system is assumed to be quasi-static in the sense that the particles which enter the interaction region at times t_0 separated by integral multiples of a wave period will execute identical trajectories. As a result, $\mathbf{v}_j(z,\mathbf{x}_{jo},t_{jo}) = \mathbf{v}_j(z,\mathbf{x}_{jo},t_{jo} + 2\pi N/\omega)$ for integer N. The discrete sum over particles can be replaced by an integration over initial conditions, and we may write Eq. (26) in the form

$$\delta \mathbf{J}(\mathbf{r},t) = -I_b \int_{A_b} dS_0\, \sigma_T(\mathbf{x}_0) \int_0^T dt_0\, \sigma_{\parallel}(t_0)\, \frac{\delta(t - \tau(z,\mathbf{x}_0,t_0))}{|v_z(z,\mathbf{x}_0,t_0)|}\, \mathbf{v}(z,\mathbf{x}_0,t_0)\, \delta(\mathbf{x} - \mathbf{x}(z,\mathbf{x}_0,t_0)), \quad (27)$$

where $I_b = n_b\, e\, v_{z0}\, A_b$ is the electronic current, A_b is the cross-sectional area of the beam and $T = L/v_{z0}$ (L = length of the interaction region), σ_T and $\sigma_{\parallel}$ describe the distribution of the initial conditions subject to the normalization

$$\int_{A_b} dS_0\, \sigma_T(r_0,\theta_0) = 1, \quad (28)$$

$$\frac{1}{T}\int_0^T dt_0\, \sigma_{\parallel}(t_0) = 1, \quad (29)$$

where $dS_0 = r_0\, dr_0\, d\theta_0$. If the electron beam has initially a non-zero emittance, then the expression (27) will also involve an average over the initial velocity distribution.

Substitution of the vector potential (Eqs. 11, 16, 23) and the source current (Eq. 27) in Eq. (10) leads to the following equation for the slowly varying amplitude and wave vector $k(z)$ which are obtained by averaging over a wave period and making use of the ortho-properties of the basis functions. For TE modes, we obtain

$$\frac{d^2 a_{ln}}{d\xi^2} + (\bar{\omega}^2 - x_{ln}^2 - \chi^2)\, a_{ln} = \frac{2e\, I_b}{\epsilon_0\, m_0\, c^3}\, H_{ln} < \frac{\beta_r\, T_l^+ + \beta_\theta\, W_l^-}{|\beta_z|} >, \quad (30)$$

$$2\chi^{1/2}\frac{d}{d\xi}(\chi^{1/2} a_{ln}) = \frac{2eI_b}{\epsilon_0\, m_0 c^3}\, H_{ln} < \frac{\beta_r\, T_l^- - \beta_\theta\, W_l^+}{|\beta_z|} >, \quad (31)$$

where

$$a_{ln} = C_{ln}\, k_{ln}\, e\, \delta A/m_0 c. \quad (32)$$

The dimensionless quantities $\bar{\omega}, x_{ln}, \chi, \beta_r, \beta_\theta, \beta_z$ and ξ in Eqs. (31) and (32) are defined as $\bar{\omega} = \omega\, r_2/c$, $x_{ln} = k_{ln} r_2, \chi = k r_2, \beta_r = v_r/c, \beta_\theta = v_\theta/c$, and $\xi = z/r_2$, respectively.

Similary, for TM modes we have

$$\frac{d^2 a_{ln}}{d\xi^2} + (\bar{\omega}^2 - x_{ln}^2 - \chi^2)\left(1 + \frac{x_{ln}^2}{\chi^2}\right) a_{ln}$$

$$= \frac{2eI_b}{\epsilon_0\, m_0\, c^3}\, H_{ln} < \frac{\beta_r\, W_l^- - \beta_\theta\, T_l^+ + (k_{ln}/k)\, Z_{ln}(k_{ln} r)\sin\Psi_l}{|\beta_z|} >, \quad (33)$$

and

$$2\left(\chi + \frac{x_{ln}}{\chi}\right)^{1/2} \frac{d}{dz}\left(\chi + \frac{x_{ln}^2}{\chi}\right)^{1/2} a_{ln}$$

$$= -\frac{2el_b}{\epsilon_0 m_0 c^3} H_{ln} <\beta_r W^+ + \beta_\theta T_l^- - (k_{ln}/k) Z_{ln}(k_{ln} r) \cos \Psi_l>. \quad (34)$$

In Eqs. (30)-(34), $H_{ln}, T_l^{\pm}$ and $W_l^{\pm}$ are mode dependent quantities defined as

$$H_{ln} = C_{ln}^2 x_{ln}^2 = \begin{cases} \dfrac{x_{ln}^2}{\pi\left[(x_{ln}^2 - l^2) Z_{ln}^2(x_{ln}) - (y_{ln}^2 - l^2) Z_{ln}^2(y_{ln})\right]}, & \text{TE mode} \\ = \dfrac{}{\pi[x_{ln}^2 Z'^2_{ln}(x_{ln}) - y_{ln}^2 Z'^2_{ln}(y_{ln})]}, & \text{TM mode} \end{cases} \quad (35)$$

where $y_{ln} = k_{ln} r_1$ and x_{ln} for TE and TM modes are solutions of Eqs. (14) and (19), respectively. Also,

$$\begin{aligned} T_l^+ &= \frac{lZ_{ln}(k_{ln} r)}{x_{ln} \bar{r}} \sin \Psi_l, \\ T_l^- &= \frac{lZ_{ln}(k_{ln} r)}{x_{ln} \bar{r}} \cos \Psi_l, \\ W_l^+ &= Z_{ln}(k_{ln} r) \sin \Psi_l, \\ W_l^- &= Z_{ln}(k_{ln} r) \cos \Psi_l, \end{aligned} \quad (36)$$

where Ψ_l is the phase slippage between the beam and the radiation field given by

$$\Psi_l = \int \chi(\xi')\, d\xi' - \frac{\bar{\omega}}{\beta_z} \xi + \frac{l \bar{\Omega}_\theta}{\beta_z} \xi, \quad (37)$$

$\bar{\Omega}_\theta = \dfrac{r_2}{c} \dfrac{d\theta}{dt}$ is the normalized azimuthal rotation frequency of the electron. Finally, the notation $< \ldots\ldots >$ describes the average of the beam electrons over the axial phase and the cross-section i.e.,

$$<F> = \frac{1}{2\pi} \int d\Psi_0\, \sigma_\Psi(\Psi_0) \int d\theta_0\, r_0 dr_0\, \sigma_T(r_0, \theta_0) F, \quad (38)$$

where $\Psi_0 = \omega t_0$. An average over the initial beam velocity distribution is also required to treat the non-zero emittance case It should be noted that average in Eq. (38) includes the overlap of the electron beam with the transverse mode structure of the radiation field and the 'filling-factor' is introduced in the theory in a self-consistent manner.

In the case of the TEM mode, we obtain

$$\frac{d^2a}{d\xi^2} + (\bar{\omega}^2 - \chi^2)\, a = \frac{eI_b}{\pi\epsilon_0\, m_0c^3 ln\left(\frac{r_2}{r_1}\right)} < \frac{r_2\beta_r}{|\beta_z|r} \cos\Psi >, \tag{39}$$

and

$$2\chi^{1/2}\, \frac{d}{d\xi}\, (\chi^{1/2}A) = -\, \frac{eI_b}{\pi\epsilon_0\, m_0c^3 ln\,(r_2/r_1)} < \frac{r_2\,\beta_r}{|\beta_z|r} \sin\,\Psi >, \tag{40}$$

where

$$a = \frac{1}{\sqrt{2\pi\, ln\,(r_2/r_1)}} \cdot \frac{e\delta A}{m_0c\; r_2}, \tag{41}$$

$$\Psi = \int \chi(\xi')d\xi' - \frac{\bar{\omega}}{\beta_z}\, \xi. \tag{42}$$

The time averaged power flow (i.e. The Poynting flux) P_ω in the waveguide can be expressed in terms of the normalized amplitude by the following relations

$$P_\omega = \frac{\pi\;\epsilon_0 m_0^2\; c^5}{2e^2} \cdot \frac{\bar{\omega}\chi}{H_{ln}} \cdot a_{ln}^2, \text{ (TE mode)}$$

$$P_\omega = \frac{\pi\;\epsilon_0\; m_0^2 c^5}{2e^2} \cdot \frac{\bar{\omega}\chi}{H_{ln}} \left[1 + \frac{x_{ln}^2}{\chi}\right] a_{ln}^2, \text{ (TM mode)}$$

$$P_\omega = \frac{\pi\epsilon_0\; m_0^2\; c^5}{e^2}\, \bar{\omega}\; \chi \cdot ln\; (r_2/r_1)\; a^2 \cdot \text{ (TEM mode)} \tag{43}$$

Although, the self-fields of the electron beam is neglected in the formulation, the nonlinear dispersion relations in Eqs. (33) and (39) include collective effects through the dielectric response of the plasma to the waveguide mode. Hence, the system will slowly evolve from a vacuum waveguide mode to a fully self-consistent dielectrically-loaded waveguide mode.

c. Orbit Equations:

The source terms in the wave equation will be calculated by solving the electron-orbit equations in the presence of the static and RF fields. Since we are considering an amplifier configuration, it is convenient to integrate the equations of motion in z and we write the Lorentz force equations in the form

$$v_z\, \frac{d\mathbf{p}}{dz} = -\, e\; (\mathbf{E}_0 + \delta\mathbf{E}_{ln}) - e\; \mathbf{v} \times \delta\; \mathbf{B}_{ln}, \tag{44}$$

where

$$\delta \mathbf{E}_{ln} = -\frac{\partial \mathbf{A}_{ln}}{\partial t} \text{ and } \delta \mathbf{B}_{ln} = \nabla \times \mathbf{A}_{ln}.$$

Substitution of the appropriate form of the vector potential yields the following normalized equation of motions for the TE_{ln} mode

$$\beta_z \frac{du_r}{d\xi} = -\frac{r_2 \hat{V}_0}{r} + \left\{ x_{ln}\, \beta_\theta\, Z_{ln}\, (k_{ln} r) \cos\Psi_l - (\bar{\omega} - \chi\beta_z)\, T_l^- \right\} a_{ln} + \beta_z\, T_l^+ \frac{da_{ln}}{d\xi} + \frac{r_2\, u_\theta^2}{\gamma r}, \tag{45}$$

$$\beta_z \frac{du_\theta}{d\xi} = -\frac{r_2\, u_r\, u_\theta}{\gamma r} + \left\{ (\bar{\omega} - \chi\beta_z)\, W_l^+ - x_{ln}\, \beta_r\, Z_{ln}\, (k_{ln} r) \cos\Psi_l \right\} a_{ln} + \beta_z\, W_l^- \frac{da_{ln}}{d\xi}, \tag{46}$$

$$\beta_z \frac{du_z}{d\xi} = -\left\{ \beta_r\, T_l^- - \beta_\theta\, W_l^+ \right\} \bar{k}\, a_{ln} - \left\{ \beta_r\, T_l^+ + \beta_\theta\, W_l^- \right\} \frac{da_{ln}}{d\xi}, \tag{47}$$

where

$$\hat{V}_0 = \frac{eV_0}{m_0 c^2} \cdot \frac{1}{ln(r_2/r_1)}. \tag{48}$$

The dimensionless quantities u_r, u_θ, and u_z are defined as $u_r = p_r/m_0 c$, $u_\theta = p_\theta/m_0 c$ and $u_z = p_z/m_0 c$, respectively.

For the TM_{ln} mode, we have

$$\beta_z \frac{du_r}{d\xi} = -\frac{r_2 \hat{V}_0}{r} + \frac{r_2 u_\theta^2}{\gamma r} + \left\{ \bar{\omega} - \beta_z\, \chi \left[1 + \frac{x_{ln}^2}{\chi^2} \right] \right\} W_l^+\, a_{ln} + \beta_z\, W_l^- \frac{da_{ln}}{d\xi}, \tag{49}$$

$$\beta_z \frac{du_\theta}{d\xi} = -\frac{r_2\, u_r u_\theta}{\gamma r} + \left\{ \bar{\omega} - \beta_z\, \chi \left[1 + \frac{x_{ln}^2}{\chi^2} \right] \right\} T_l^-\, a_{ln} + \beta_z\, T_l^+ \frac{da_{ln}}{d\xi}, \tag{50}$$

$$\beta_z \frac{du_z}{d\xi} = \left\{ \left[\chi + \frac{x_{ln}^2}{\chi} \right] (\beta_\theta\, T_l^- + \beta_r\, W_l^+) - \frac{\bar{\omega}\, \chi_{ln}}{\chi}\, z_{ln}\, (k_{ln} r) \cos\Psi_l \right\} a_{ln} - \beta_z\, (\beta_r\, W_l^- - \beta_\theta\, T_l^+) \frac{da_{ln}}{d\xi}. \tag{51}$$

For the TEM mode, we obtain

$$\beta_z \frac{du_r}{d\xi} = -\frac{r_2 \hat{V}_0}{r} + (\bar{\omega} - \beta_z \chi) \frac{r_2 \sin\Psi}{r}\, a + \frac{r_2 \cos\Psi}{r} \cdot \frac{da}{d\xi} + \frac{r_2 u_\theta^2}{\gamma r}, \tag{52}$$

$$\beta_z \frac{du_\theta}{d\xi} = -\frac{r_2 u_r u_\theta}{\gamma r}, \tag{53}$$

$$\beta_z \frac{du_z}{d\xi} = r_2 \beta_z \left\{ \frac{\chi \sin\Psi}{r} a - \frac{\cos\Psi}{r} \frac{da}{d\xi} \right\}. \tag{54}$$

In addition, we have for all modes

$$\beta_z \frac{d\zeta}{d\xi} = U_r/\gamma, \tag{55}$$

$$\beta_z \frac{d\theta}{d\xi} = U_\theta/\gamma\zeta \tag{56}$$

From Eqs. (37) and (42) we also have

$$\frac{d\Psi_l}{d\xi} = \chi + \frac{l\bar{\Omega}_\theta}{\beta_z} - \frac{\bar{\omega}}{\beta_z}, \text{ (TE and TM modes)} \tag{57}$$

and

$$\frac{d\Psi_l}{d\xi} = \chi - \bar{\omega}/\beta_z \text{ (TEM mode)} \tag{58}$$

where $\zeta = r/r_2$. Both the linear and the nonlinear evolution of the orbitron amplifier are included in the formulation through Eqs. (30)-(42) for the fields and Eqs. (45)-(58) for the particles. For particle motion in equilibrium circular orbits, the synchronous condition for the beam-wave interaction is $\bar{\omega} = \chi\beta_z + l\bar{\Omega}_\theta$. Under this condition, $\frac{d\Psi_l}{d\xi} = 0$ from Eq. (57). Hence, Ψ_l is a slowly varying function of z near synchronism. For eccentric orbits, however, the synchronism occurs,[7] when $\bar{\omega} = \chi\beta_z + l\bar{\Omega}_\theta + s\bar{\Omega}_r$ and $\frac{d\Psi_l}{dz} \neq 0$. This results in rapid variation of Ψ with z. For TEM mode, the interaction occurs only with eccentric orbits as mentioned before. In the numerical solution of the differential equations, a smaller step-size will be required for the eccentric orbits in comparison to that for the circular orbits to resolve the rapid variation of Ψ with z.

III. NUMERICAL SIMULATION

The set of coupled differential equations derived in Sec. II is solved numerically. In the amplifier configuration, a single wave of frequency ω is injected into the system at $z = 0$. The Maxwell's Eqs (30-31), Eqs (33-34) and Eqs (39-40) can be converted to a set of three first order differential equations in a, $da/d\xi$ and χ. Hence, the system of equations to be solved consists of $6N_l + 3$ first order ordinary differential equations, where N_l is the total number of electrons. We employ the modified

version (Gill's method) of the fourth-order Runge-Kutta algorithm for numerical solution of the differential equations. The average of the form shown in Eq. (38) which occur in the Maxwell's equations are performed by means of an N-*th* order Gaussian quadrature techniques in each of the variables r_0,θ_0,Ψ_0. Hence, $N_T = N^3$. For the examples shown in this section, a choice of $N = 10$ is found to provide an accuracy of better than 0.1%.

The initial conditions on the radiation field are chosen such that $da/d\xi = 0$ at $z = 0$ and $\chi(z = 0) = \sqrt{\bar{\omega}^2 - x_{ln}^2}$ with $x_{ln} = 0$ for the TEM mode. The initial amplitude $a(z = 0)$ is calculated from the input signal power using Eqs. (43). The initial state of the electrons is chosen to model the injection of an axisymmetric, monoenergetic beam of zero emittance. The non-zero emittance effects can, however, be included in a straight-forward manner but requires the injection of a very large number of particles to sample the initial velocity distribution. We assume that the beam has an uniform distribution i.e., $\sigma_{\Psi_0}(\Psi_0) = 1$ in the range $0 \leqslant \Psi_0 \leqslant 2\pi$. We will consider two different forms of the transverse distribution function $\sigma_I(r_0,\theta_0)$ depending on the mode of the injection of the beam. When the beam is injected into the steady-state circular orbits, we assume a uniform cross-sectional distribution i.e., $\sigma_{r_0}(r_0,\theta_0) = 1/A_b$ for $0 \leqslant \theta_0 \leqslant 2\pi$ and $R_{min} \leqslant r_0 \leqslant R_{max}$. For injection into eccentric orbits, we use the distribution assumed in Ref. (7)

$$\sigma_{r_0}(r_0) \propto \frac{1}{r_0} \cdot \frac{1}{\sqrt{H_0 - \dfrac{P_\theta}{2m_0 r_0^2} - \dfrac{P_z^2}{2m_0} - \dfrac{eV_0}{\ln(r_2/r_1)} \ln \dfrac{r_0}{r_1}}}, \tag{59}$$

for $r_{in} \leqslant r_0 \leqslant r_{out}$ and uniform in θ_0 in the range 0 to 2π. In addition, we have to specify the applied d.c. voltage V_0, the beam current I_b, $H_0 = eV_b$ (beam energy), P_{z0} (initial axial momentum) and P_{θ_0} (initial angular momentum). Sometimes, it is more convenient to specify $\sigma = r_{out}/r_{in}$, $\alpha = P_{\perp 0}/P_{z0}$ and r_{out} in stead of H_0, P_{z0} and P_{θ_0}. In the nonrelativistic case, the following relations hold between these two sets of parameters as derived by Burke et al[7]

$$\begin{aligned} P_\theta &= r_{out}\left[\frac{2m_0 eV_0}{\ln(r_2/r_1)} \cdot \frac{\ln\sigma}{\sigma^2 - 1}\right]^{1/2}, \\ P_z &= \sqrt{2m_0 H_0 - P_\theta^2} = \sqrt{2mH_0/(1+\alpha^2)}, \\ H_0 &= \frac{1+\alpha^2}{\alpha^2} \cdot \frac{eV_0}{\ln(r_2/r_1)} \cdot \left[\ln \frac{r_{out}}{r_1} + \frac{\ln\sigma}{\sigma^2 - 1}\right] \end{aligned} \tag{60}$$

In the limit $\sigma \rightarrow 1$ (i.e., circular orbits) the term $\frac{ln\sigma}{\sigma^2-1} \rightarrow \frac{1}{2}$. Here $P_\perp$ is the magnitude of the transverse component of the momentum.

The neglect of the space charge effects can be justified if the current I_b is less than

$$I_b << 2\pi\epsilon_0 c\beta_z \frac{V_0}{ln(r_2/r_1)}$$

so that the maximum electric field of an annular beam of electrons is small compared to the applied electric field. A restriction also applies on the bias voltage V_0. To avoid the break-down condition, $V_0 < E_{bk} r_1 ln\frac{r_2}{r_1} = 100 r_1$ (in cm) $ln\frac{r_2}{r_1}(kV)$, where E_{bk} ($\sim$ 100 kV/cm) is the break-down field. For a given r_2, the factor $r_1 ln\frac{r_2}{r_1}$ attains a maximum value of r_1 when $ln\frac{r_2}{r_1} = 1$ (i.e., $r_1 = r_2/2.718$). The rotational frequency Ω_μ of the electrons in circular orbits should satisfy the condition $f_\mu = \frac{\Omega_\mu}{2\pi} < \frac{1}{2\pi r_0}\sqrt{\frac{e}{m_0}E_{bk} r_1} < \frac{1}{2\pi}\sqrt{\frac{e}{m_0 r_1}E_{bk}} \simeq \frac{2.112}{\sqrt{r_1(\text{in cm})}}$ (GHz). Hence r_1 is very small for high frequency operation. As a result, V_0 (and H_0 in Eq. 60) will be small unless the ratio r_2/r_1 is large. For example, $r_1 < 0.00364$ cm for $f_\mu = 35$ GHz and $r_2/r_1 > 8.5 \times 10^{11}$ to get $V_0 \simeq 10$ kV. Such a large value of r_2/r_1, however, decreases the overlap integrals between the electron orbits and the transverse mode structure of the radiation field with a consequent reduction in the interaction strength. Thus, high frequency, high efficiency operation of the orbitron amplifier in the fundamental mode is not feasible. A larger value for r_1 can be utilized by operating at higher harmonics of Ω_μ and higher order radiation modes but a slotted inner conductor i.e., magnetron-type structure will be required to increase the interaction efficiency. The slotted wave guide structure will be discussed in a subsequent paper.

We now show the results of our calculations for the two lowest order modes, namely TE_{11} and TEM. We first consider the TE_{11} mode propagation with electron injection in steady-state circular orbits. The evolution of the waveguide mode is shown in Fig. 2. The frequency of the wave is $\omega/ck_{zn} = 1.06$ (2.317 GHz) and the input power is 0.01W. The inner and outer radii of the conductors are, respectively, 0.2 cm and 4.0 cm. The cut-off frequency (f_{cut}) is 2.186 GHz. The initial radius, r_0 of the electron beam is taken as 0.426 cm and the position (θ_0, Ψ_{j0}) were chosen by a 10-point Gaussian weighting. The d.c. voltage V_0 between two conductors is 53.7 kV. The beam voltage V_b = 32.5 kV is

found from Eq. (60) for $\alpha = 1.5$ and $\sigma = 1$. The beam current I_b is 0.5 A and the beam power $P_b = 16.25$ kW. The growth of the wave mode is approximately exponential after an initial transient region $k_{ln} z \leqslant 30$. During the linear phase of the interaction the growth rate $\Gamma = \frac{1}{a_{ln}} \frac{d}{dz} a_{ln}$ is 0.16 dB/cm, and an increase is observed prior to saturation at $k_{ln} z \simeq 124.0$. The radiation power at saturation is 1008 W for an efficiency of $\eta = 6.2\%$. The electron bunching is very weak in the orbitron. This is seen from the simulation of the distribution of the electons in real space as well as in momentum space at various axial positions. The radiation power grows mostly at the expense of the potential energy of the electrons. The particles move to lower values of r causing an increase in the orbital frequency. As a result, the electrons fall out of resonance quickly and the power saturates at a low level yielding a small efficiency.

The efficiency at saturation (η_{peak}) versus frequency is shown in Fig. 3 for different values of $V_0 = 51.5$, 53.7, 56.0 and 59.0 kV with the other parameters being the same as in Fig. 2. The beam voltages corresponding to the above values of the d.c. voltage are respectively, 31.19, 32.52, 33.92 and 35.7 kV. In curve (a) of Fig. 3, the beam line intersects the waveguide dispersion curve at two frequencies resulting in a broad-band response. The bandwidth at half-maximum is about 10%. The other three curves represent below 'grazing condition' (beam line and dispersion curve are tangetial). The peak efficiency attains the highest value ($\eta_{peak} \sim 6.6\%$) below grazing at $V_0 = 51.5$kV. The efficiency decreases very rapidly to zero as V_0 goes below 51.5 kV. For $V_0 > 51.5$kV also, η decreases but slowly to 5.4% at $V_0 = 59$kV. The bandwidth, however, increases as V_0 rises above 51.5 kV. Although, η increases as the beam line moves below grazing, the growth rate decreases as can be inferred from Fig. 4 where the interaction length corresponding to η_{peak} is plotted as a function of frequency for the various cases considered in Fig. 3. The efficiency was not calculated for $V_0 > 59.0$kV, since the beam line intersects the backward wave region of the dispersion curve. These characteristics of the orbitron are in common with the other fast wave devices such as gyrotron and FEI.

The variation of the efficiency with beam energy is shown in Fig. 5 where η versus frequency is plotted at different values of V_b. The parameters V_0, r_2, r_1 and r_0 are chosen such that the beam line is above grazing in each case. The efficiency is not a sensitive function of the beam energy. The efficiency increases from 4% to 6% as V_b increases from 10 kV to 60 kV.

We now turn to the case of the TEM mode. In this case, the numerical simulation models an electron beam injected at $z=0$ into elliptic orbit with eccentricity $\sigma = 5$. The complete spectrum of efficiency versus frequency is shown in Fig. 6 for two values of $V_b = 10$ kV and 10.64 kV. Other parameters chosen are $r_2 = 5.0$ cm, $r_1 = 0.05$ cm, $V_0 = 13.5$ kV, $I_b = 0.5A$, $\alpha = 1.5$. The input signal power is 0.01 W. The outer turning points for the two values of V_b are found from Eq. (60) to be $r_{tp} = 0.496$ cm and 0.577 cm, respectively. The peak efficiency $\eta_{peak} \simeq 5.04\%$ with a bandwidth of 3.5%. The frequency (ω_{peak}) for peak efficiency is a sensitive function of the beam voltage as seen from Fig. 6 where $\omega_{peak} r_2/c$ shifts from 2.075 to 1.775 as V_b increases from 10 kV to 10.69 kV. The growth rate at $\omega r_2/c = 2.075$ (1.952 GH) is $\Gamma r_2 = 0.52$ (0.9 dB/cm).

The efficiencies of the TE_{11} and TEM modes are comparable but the bandwidth is larger for the TE_{11} mode. The growth rate, however, is higher for the TEM mode. The TEM mode has the disadvantage of having no cut-off frequency and resonant interaction occurs with both forward and backward waves. Special methods[7] have to be adopted to suppress the backward wave oscillations.

The bunching of the electron beam and the efficiency of the interaction may be improved greatly by using a slotted inner conductor[2] (i.e., magnetron-type structure) in the coaxial waveguide. The large gradient of the E-field in such a structure may focus the axis encircling beam to the decelerating region of the radiation fields and maintain bunching over a longer interaction length. The slotted structure has the further advantage of operation at higher harmonics of the orbital frequency.

IV. SUMMARY AND DISCUSSION

We have developed a self-consistent three-dimensional theory of the orbitron maser in the amplifier configuration with an axially injected beam in a coaxial waveguide with circular cross-section. The theory has been developed for all modes of polarization (TE, TM, TEM) of the radiation field and for electron orbits with arbitrary eccentricity. The saturation efficiency of the orbitron in its simplest form is found to be small. The efficiency (η) for the TE_{11} mode is about 6% with $V_0 = 53.7$ kV, $V_b = 32.5$ kV and $I_b = 0.5$A, while the growth rate in the linear region is 0.16 dB/cm. The efficiency decreases to 4.5% at lower values of $V_0 = 15.7$ kV and $V_b = 9.33$ kV for a growth rate of 0.14 dB/cm. The efficiency for TEM mode is comparable to that of the TE mode but the growth rate is higher. For the

TEM mode, $\eta \simeq 4.0\%$ with $V_0 = 13.5$ kV, $V_b = 10$kV and $I_b = 0.5A$. The growth rate is 0.9 dB/cm. The TEM mode, however, has the disadvantage of having no cut-off frequency and resonant interaction leads to excitation of both forward and backward waves. In the case of the TE or TM mode, the physical parameters can be chosen so that only forward wave amplification occurs. Careful design will be necessary to suppress the backward wave oscillation in TEM mode.

Since the bunching of the beam is very small in the present form of the orbitron amplifier, methods have to devised to improve the bunching and the efficiency of the interaction. The use of a slotted inner conductor may enhance the bunching due to focussing action of the large gradient in the E-field in such a configuratioon. Another way of maintaining the beam-wave resonance over longer interaction length is to taper the inner conductor i.e., reduce the radius along the axis so that orbital frequency of the electron remains constant as its radius decreases due to loss of energy.

The results in this paper have been calculated for frequencies in the range 1 GHz to 10 GHz by considering the interaction with the fundmental orbital frequency. With an axially injected beam, the interaction in the fundmental orbital frequency is not suitable for the generation of high power, high frequency radiation because of two contradicitory requirements. The radius of the inner conductor should be very small for high frequency but a larger radius is required to keep the electric field below the breakdown limit when a high d.c. voltage is applied between the two conductors. High frequency radiation may be generated by utilizing resonance with the higher harmonics of the orbital frequency. This may be achieved either by using eccentric orbits in 'smooth bore' coaxial waveguide [7] or by using circular orbits in a coaxial guide with a slotted inner conductor. In the first method, the efficiency is not expected to be higher then in the fundamental. An enhancement of efficiency is expected in the second method for reasons stated earlier. The second alternative will be investigated in a future publication.

ACKNOWLEDGMENT

The authors are grateful to Dr. R.K. Parker and Dr. S.Y. Park for many helpful discussions. The work was supported by the Office of Naval Research.

REFERENCES

1. D.A. Watkins and G. Wada, Proc IRE **46**, 1700 (1958).

2. I. Alexeff and F. Dyer, Phys. Rev. Lett. **45** 351 (1980).

3. R.H. Pantell, IRE Trans. on Electron Devices, **ED-7**, 22 (1960).

4. Y.Y. Lau and D. Chernin, Phys. Fluids **27**, 2319 (1984)

5. Y.Y. Lau and D. Chernin, Phys. Rev. Lett. **52**, 1425 (1984)

6. I. Alexeff, Phys. Fluids, **28**, 1990 (1985)

7. J.M. Burke, W.M. Manheimer, and E. Ott, Phys. Rev. Lett. **56**, 2652 (1986)

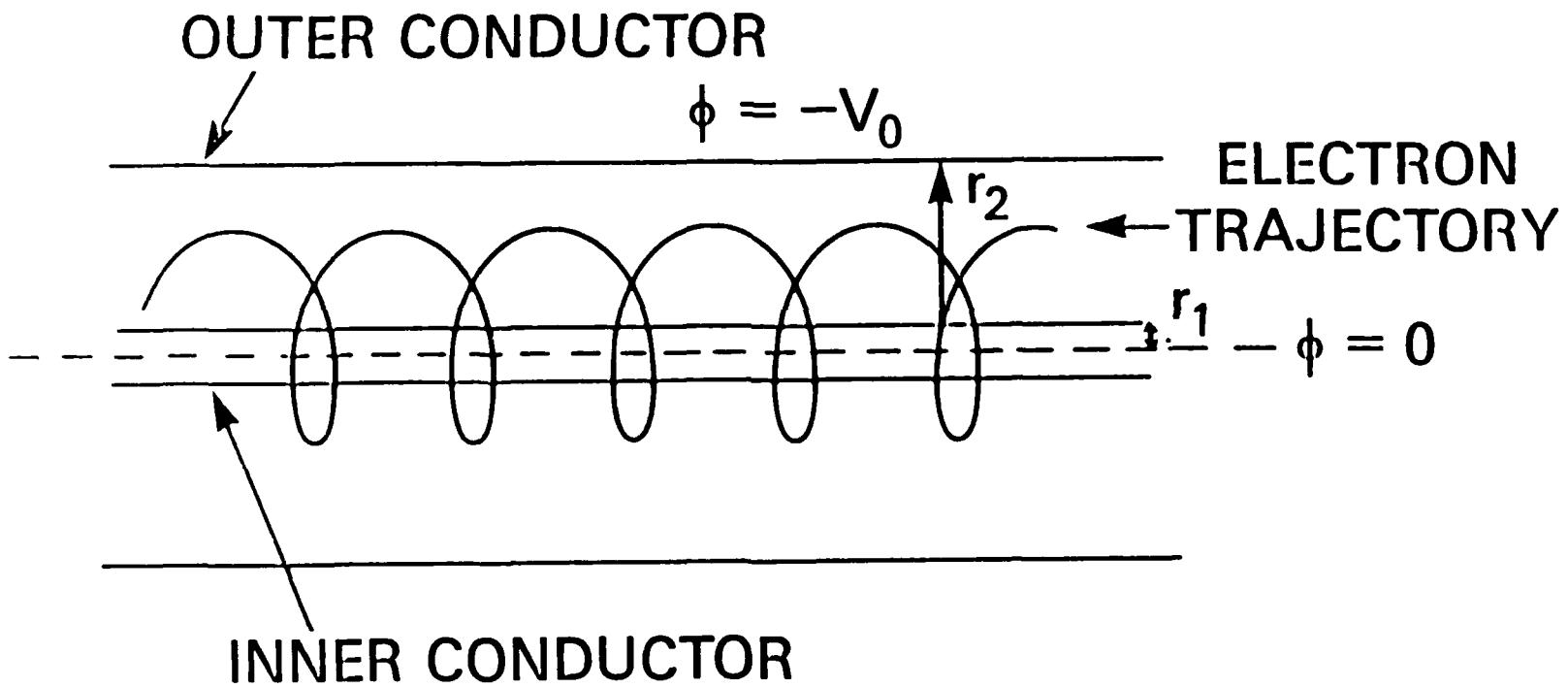

Fig. 1 — Orbitron Maser configuration

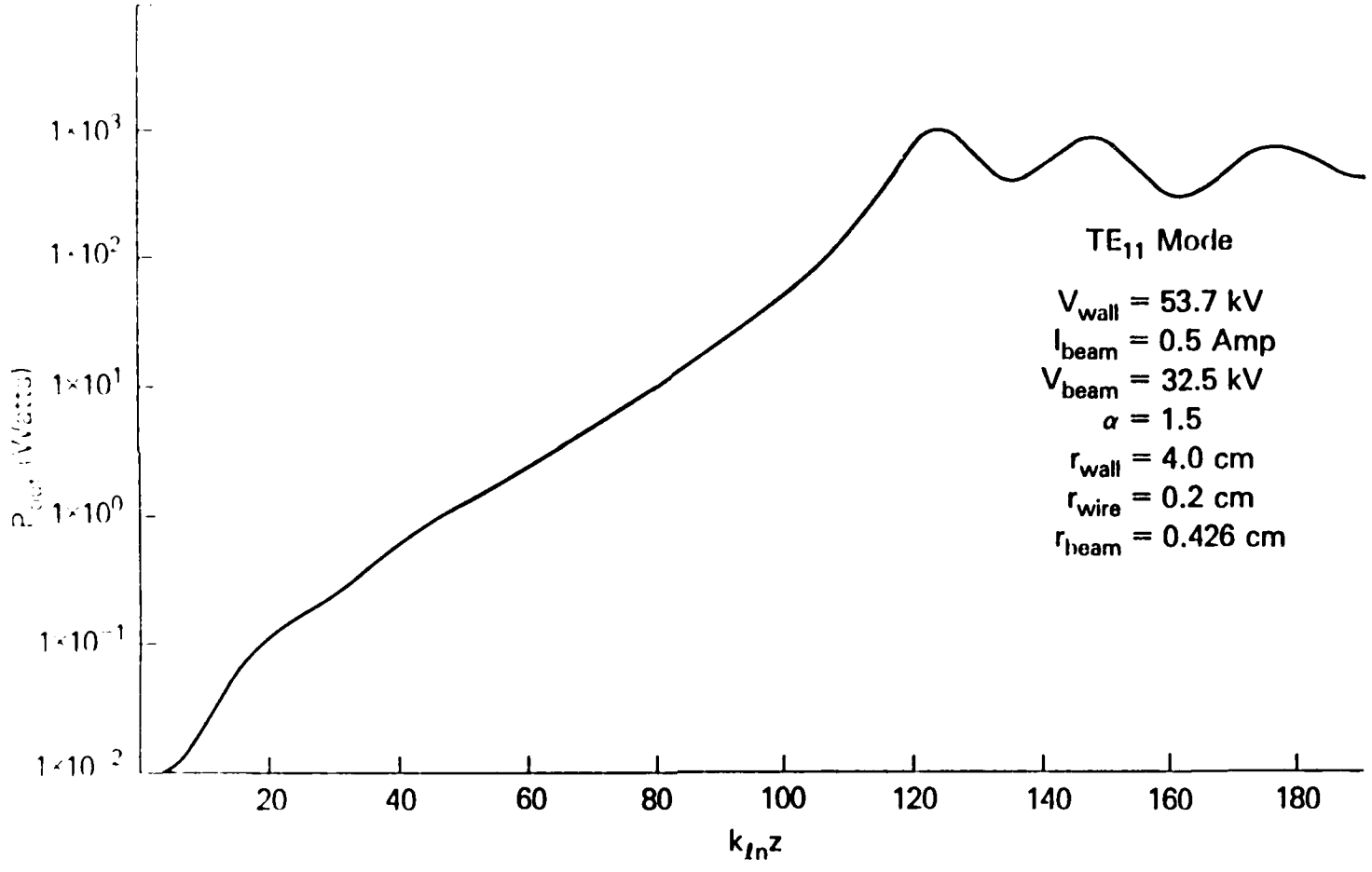

Fig. 2 — Evolution of (a) radiation power and (b) growth rate for TE_{11} mode as functions of axial positions. Parameters are: $\sigma = 1$, $\alpha = 1.5$, $f = 1.06\ f_{cut}$, $r_2 = 4$ cm, $r_1 = 0.2$ cm, $r_0 = 0.426$ cm, $I_b = 0.5$A, $V_b = 32.52$ kV and $V_0 = 53.7$ kV. Input signal power is 0.01 W.

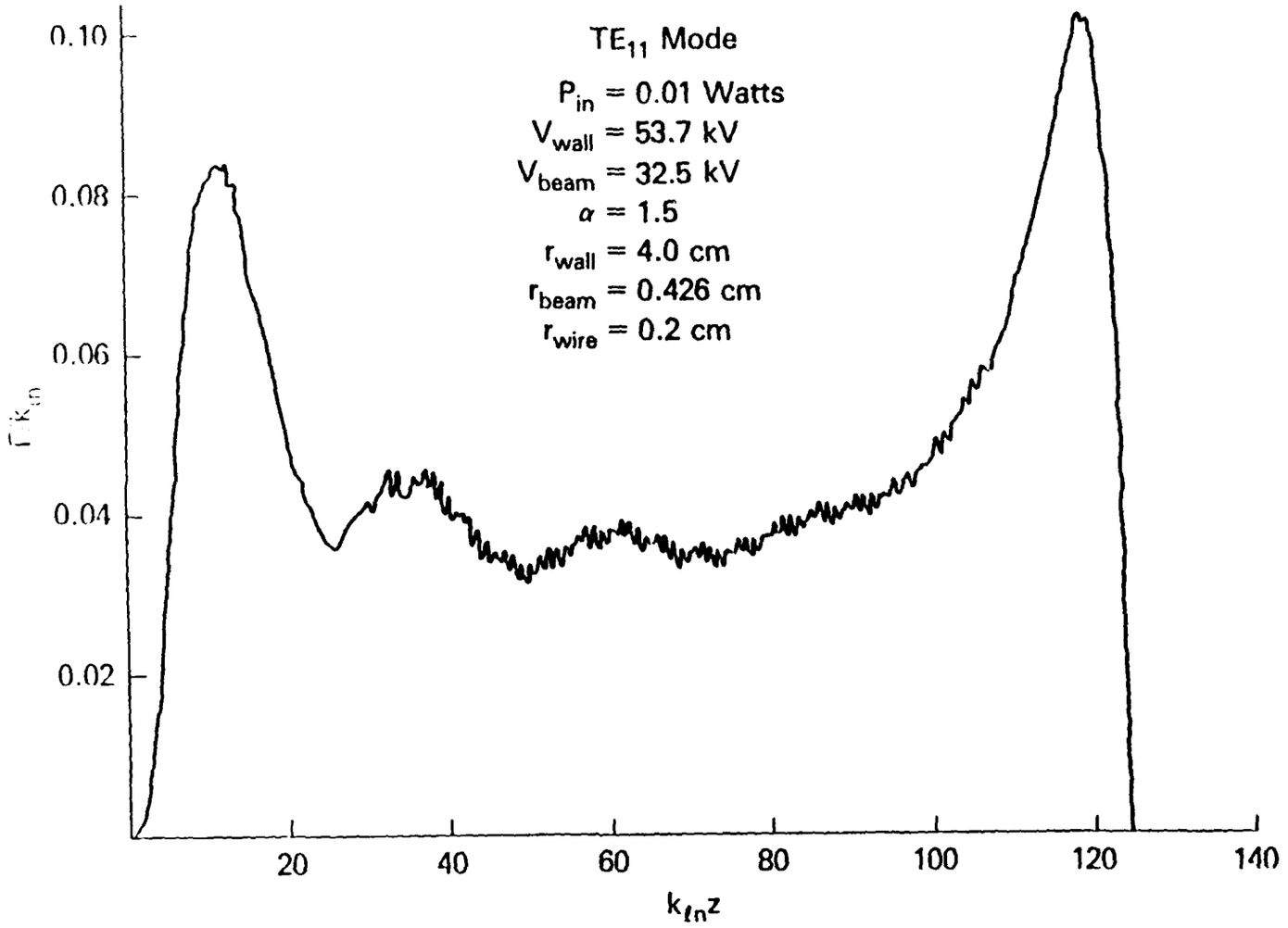

Fig. 2 (Cont) — Evolution of (a) radiation power and (b) growth rate for TE_{11} mode as functions of axial positions. Parameters are: $\sigma = 1$, $\alpha = 1.5$, $f = 1.06\ f_{cut}$, $r_2 = 4$ cm, $r_1 = 0.2$ cm, $r_0 = 0.426$ cm, $I_b = 0.5$A, $V_b = 32.52$ kV and $V_0 = 53.7$ kV. Input signal power is 0.01 W.

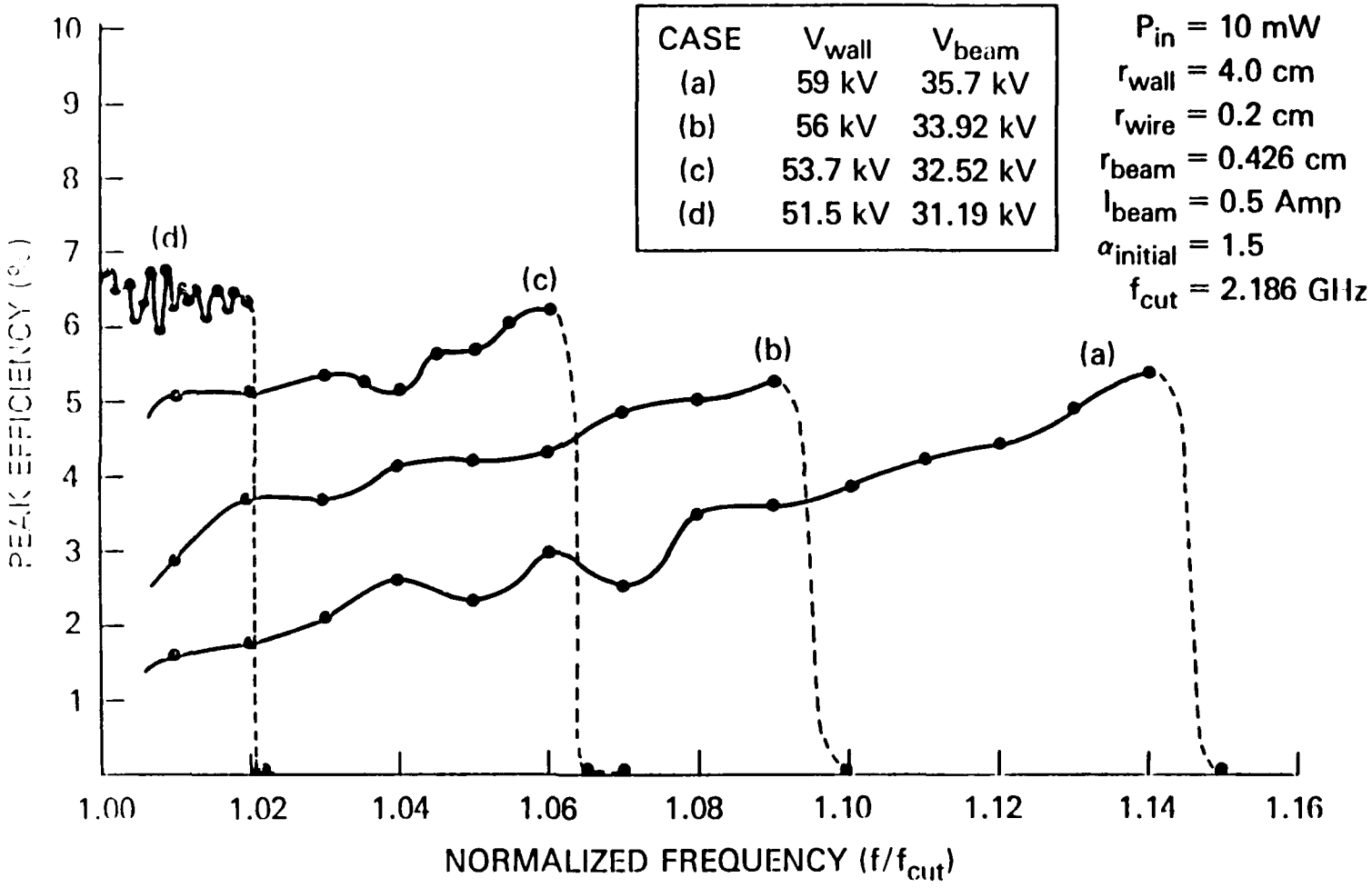

Fig. 3 — Peak efficiency versus frequency for four different values of V_0 = 51.5 kV, 53.7 kV, 56 kV and 59 kV. The corresponding values of beams voltage V_b are 31.19, 32.52, 33.92 and 35.7 kV, respectively. Other parameters: r_2 = 4 cm, r_1 = 0.2 cm, r_0 = 0.426 cm, σ = 1, α = 1.5, I_b = 0.5A and P_{IN} = 0.01W.

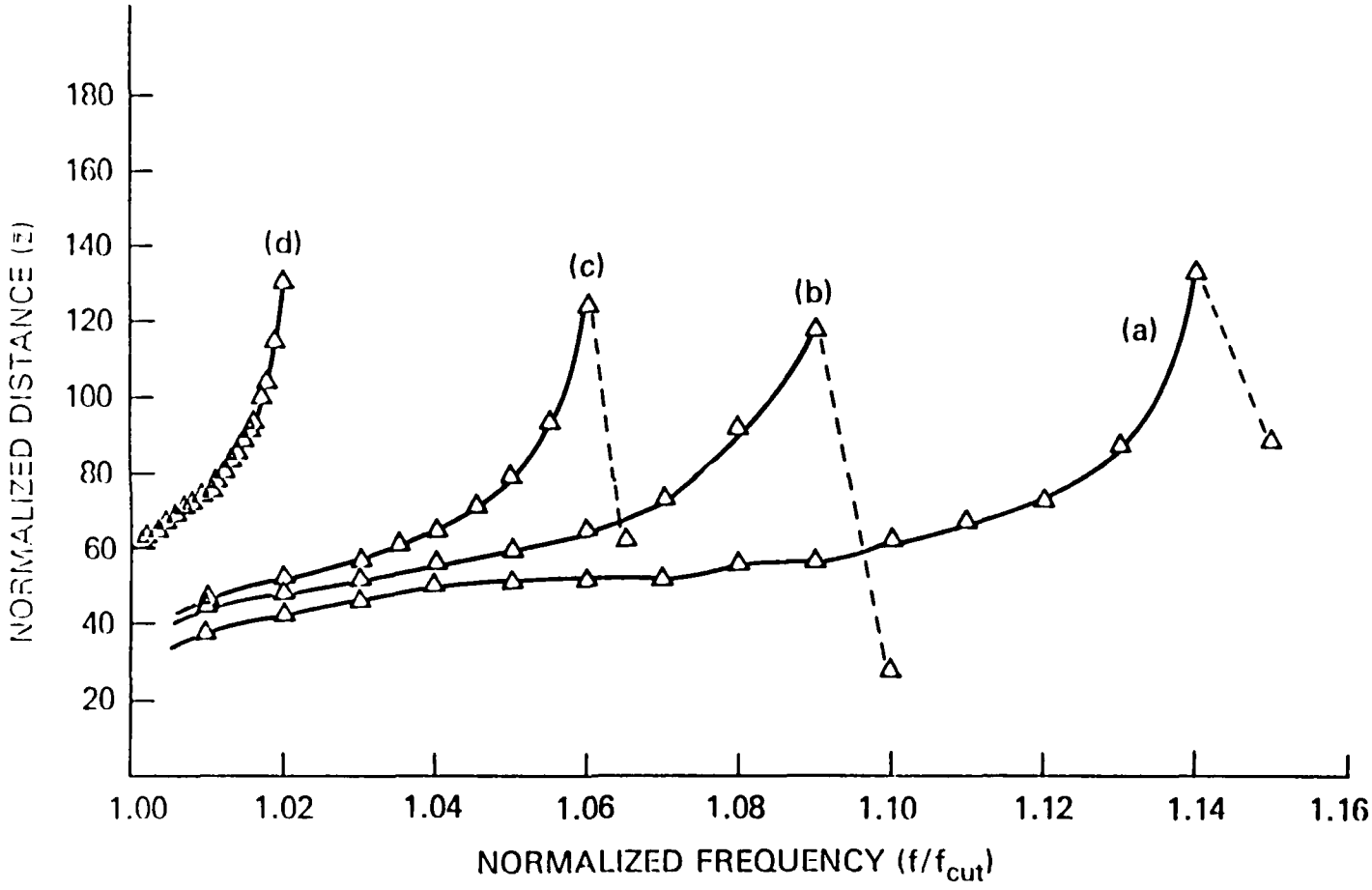

Fig. 4 — The interaction lengths corresponding to the peak efficiencies in Fig. 3 vs frequency. Parameters are the same as in Fig. 3.

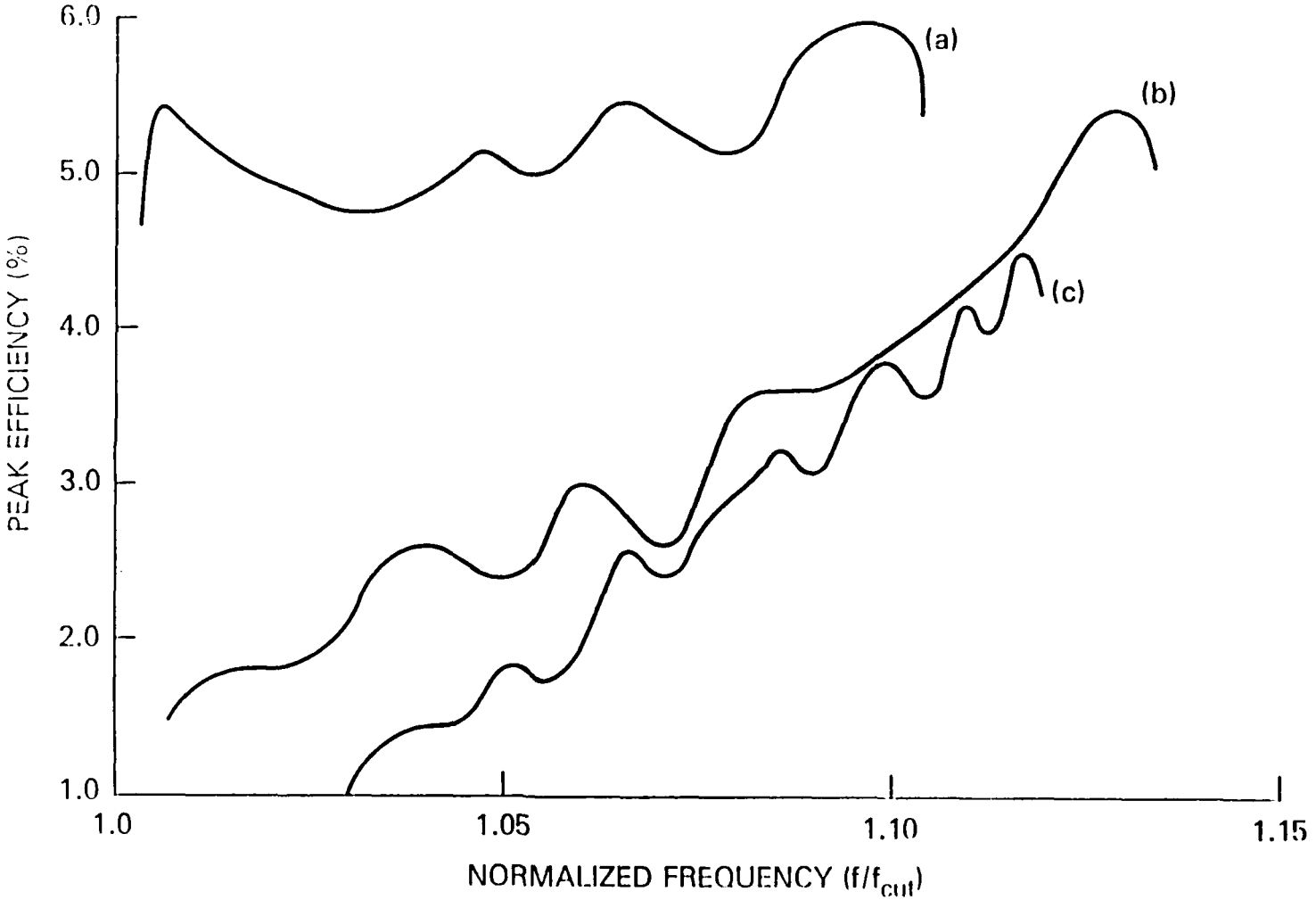

Fig. 5 — Peak efficiency vs frequency for three different values of beam energy. Curve (a): $V_b = 65.0$ kV, $V_0 = 97.4$ kV, $r_2 = 4.94$ cm, $r_1 = 0.38$ cm, $r_0 = 0.76$ cm, $f_{cut} = 1.758$ GHz; curve (b): $V_b = 35.7$ kV, $V_0 = 59.0$ kV, $r_2 = 4$ cm, $r_1 = 0.2$ cm, $r_0 = 0.426$ cm, $f_{cut} = 2.186$ GHz; curve (c): $V_b = 9.8$ kV, $V_0 = 16.5$ kV, $r_2 = 4$ cm, $r_1 = 0.05$ cm, $r_0 = 0.184$ cm, $f_{cut} = 2.197$ GHz. For all cases $\alpha = 1.5$, $I_b = 0.5$A and $P_{IN} = 0.01$ W.

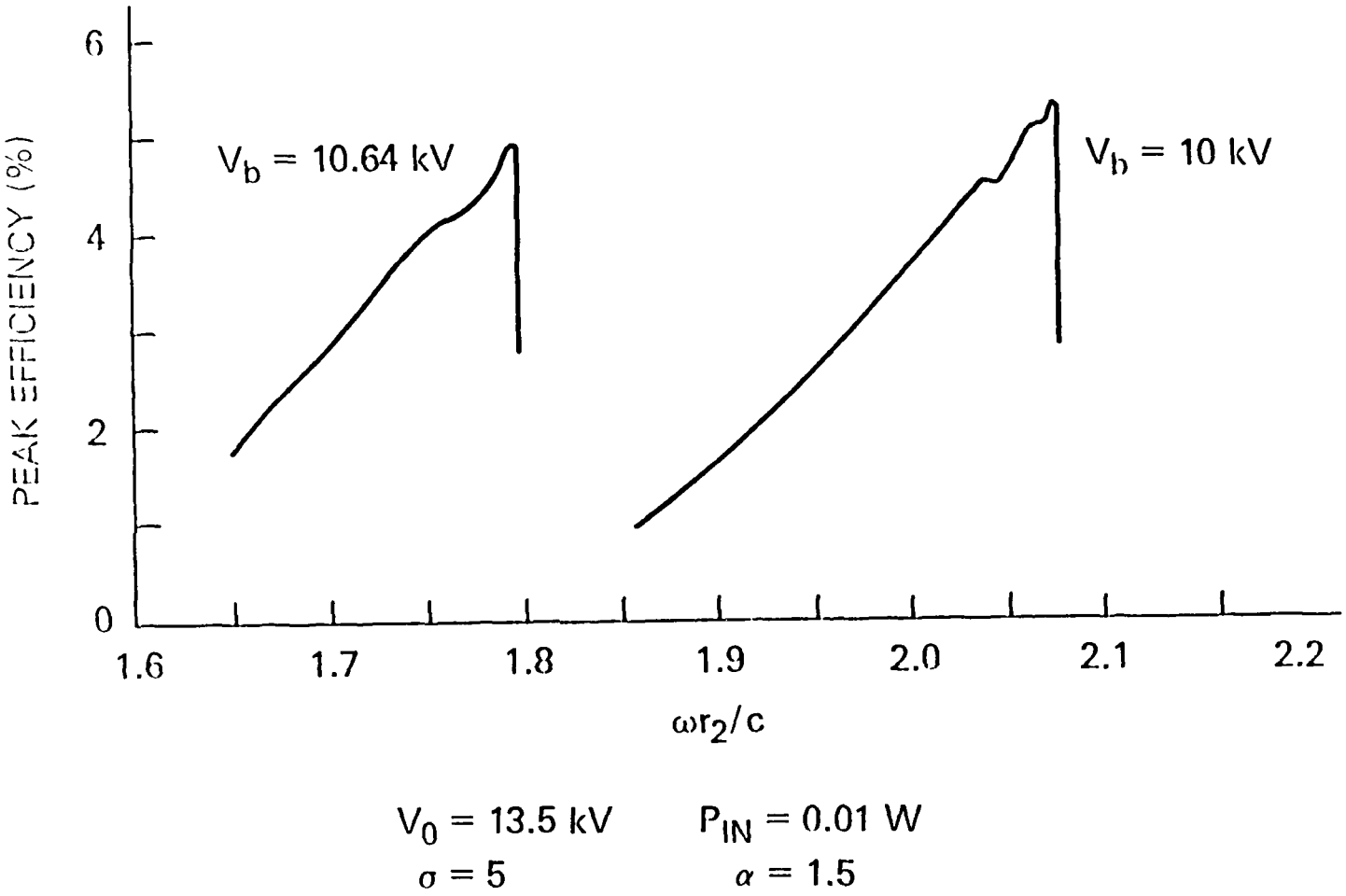

Fig. 6 — Peak efficiency vs. frequency for the TEM mode at V_b = 10.0 kV (curve a) and 10.64 kV (curve b). Other parameters are: σ = 5, V_0 = 13.5V, I_b = 0.5A, α = 1.5, σ = 5, r_1 = 0.05 cm and r_2 = 5 cm.

END

9-87

DTIC